12 Quantum Chemistry on Quantum Computers

Libor Veis

J. Heyrovský Institute of Physical Chemistry
Academy of Sciences of the Czech Republic, v.v.i.
Dolejškova 3, 18223 Prague 8, Czech Republic

Contents

1 Introduction

An exact simulation of quantum systems, including those in quantum chemistry, on a classical computer is computationally hard. The problem lies in the dimensionality of the Hilbert space needed for the description of a studied system that in fact grows exponentially with the size of this system, which is illustrated in Fig. 1. No matter if we simulate the dynamics or calculate some static property, e.g. the energy, this limitation is always present. Richard Feynman came up with an alternative to the classical simulation [1]. His idea was to convert the aforementioned drawback of quantum systems into their benefit. He suggested to map the Hilbert space of a studied quantum system on another one (both of them being exponentially large) and thus to *efficiently* simulate one quantum system on another one (i.e. on a quantum computer).

Although developing small quantum computers has taken over 30 years, we may soon benefit from Feynman's suggestion.[1] Indeed, quantum chemistry is supposed to be one of the first practical applications of small noisy quantum computers, named noisy intermediate-scale quantum (NISQ) devices [4]. Moreover, it is believed that quantum computers will eventually allow us to tackle classically intractable problems in chemistry, physics, and materials science [5–7]. In particular, *strongly correlated systems*, such as catalysts or high temperature superconductors, belong to problems of high socio-economic importance, which might be solved with the help of quantum hardware.

So far, several quantum algorithms have been proposed to solve computationally hard problems in chemistry *efficiently* (i.e. in polynomial time with polynomial resources with respect to size of the studied system and accuracy). Some of them have also been demonstrated experimentally [6]. However, due to limited quantum hardware capabilities, these experiments represent "only" proof-of-principle simulations of small chemical systems, which we can easily simulate classically. In order to make them scalable, there is a need for quantum error correction, which requires lower error rates than are currently available and moreover orders of magnitude more (physical) qubits. This field, on the other hand, grows very rapidly and we might see error-corrected digital quantum simulations of molecules in not so far future.

As mentioned above, several quantum algorithms which can solve different kinds of problems in chemistry have already been proposed [6]. In fact, quantum computational chemistry [5] has achieved enormous progress in the last 15 years.[2] In this chapter, we mention some of the algorithms, but most of the time restrict ourselves to the electronic structure problem of molecular Hamiltonians, i.e., the problem of finding the low lying energy spectrum of molecules. These algorithms can serve as subroutines for geometry optimization, calculation of optical properties, or determination of reaction rates [5]. Moreover, the methodology elaborated here can be easily applied to other problems (e.g. vibrational analysis). We focus on digital quantum simulation (analog quantum simulation is a subject of a different chapter), which means that the

---

[1]In fact, quantum computers with more than about 50 qubits are supposed to outperform the largest classical supercomputers and the first papers presenting the so called *quantum supremacy* have already appeared [2, 3]. However, the problems which they solved are rather artificial and not directly usable in chemistry simulations.

[2]The pioneering work of Aspuru-Guzik *et al.* [8] is being considered as the beginning of the quantum computational chemistry.

$$100 \qquad\qquad \approx 10^7 \qquad\qquad \approx 10^{46}$$
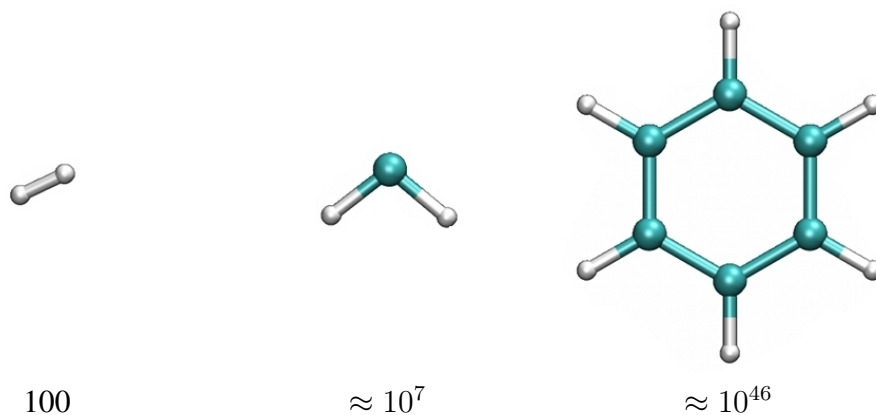
Fig. 1: *Exponential scaling of the Hilbert space dimension demonstrated on the examples of H_2, CH_2, and C_6H_6 molecules. The numbers below the molecular structures represent the number of Slater determinants in the full configuration interaction method (exact diagonalization) in double-ζ basis.*

original problem is mapped on a set of (quantum) gates which can be implemented on an universal quantum computer (i.e. not purpose specific). The chapter is meant to be a pedagogical introduction. For more details and references to original papers, we refer readers to the recent extensive reviews [5,6], from which we also draw a lot of information.

The chapter is organized as follows: we start with the basic elements of quantum computing in Sec. 2 and quantum chemistry in Sec. 3. We are aware of the fact that these topics are covered also in other chapters, however to make this chapter self-contained, we very briefly mention the basics, which are necessary for subsequent discussion of quantum algorithms for chemistry. In Sec. 4, we describe how to map the quantum chemistry problems onto a register of qubits (both in first and second quantization) and in Sec. 5 we present quantum algorithms for chemistry, both for the ultimate error-corrected applications (phase estimation, Sec. 5.1) as well as for NISQ devices (variational quantum eigensolver, Sec. 5.2). We end up with conclusions in Sec. 6.

2 Quantum computing in a nutshell

2.1 Qubit-based circuit model

We work with the qubit-based circuit model of quantum computation [9]. Similarly as the fundamental entity of classical computation and classical information is one bit, the fundamental entity of quantum computation and quantum information is one qubit. It is a quantum two-state system in a normalized state

$$|\psi\rangle = \alpha|0\rangle + \beta|1\rangle, \qquad |\alpha|^2 + |\beta|^2 = 1, \tag{1}$$

where α and β are complex-valued amplitudes. The orthonormal computational basis $\mathcal{B} = \{|0\rangle, |1\rangle\}$ is defined as

$$|0\rangle = \begin{pmatrix} 1 \\ 0 \end{pmatrix}, \quad |1\rangle = \begin{pmatrix} 0 \\ 1 \end{pmatrix}, \quad \text{therefore} \quad |\psi\rangle = \begin{pmatrix} \alpha \\ \beta \end{pmatrix}. \tag{2}$$

When going to n qubits, the system is described by a vector from the 2^n dimensional Hilbert space, which is formed by the tensor product of the Hilbert spaces of individual qubits. For example, a two-qubit system has four computational basis states

$$|00\rangle = \begin{pmatrix} 1 \\ 0 \end{pmatrix} \otimes \begin{pmatrix} 1 \\ 0 \end{pmatrix} = \begin{pmatrix} 1 \\ 0 \\ 0 \\ 0 \end{pmatrix}, \qquad |01\rangle = \begin{pmatrix} 1 \\ 0 \end{pmatrix} \otimes \begin{pmatrix} 0 \\ 1 \end{pmatrix} = \begin{pmatrix} 0 \\ 1 \\ 0 \\ 0 \end{pmatrix},$$

$$|10\rangle = \begin{pmatrix} 0 \\ 1 \end{pmatrix} \otimes \begin{pmatrix} 1 \\ 0 \end{pmatrix} = \begin{pmatrix} 0 \\ 0 \\ 1 \\ 0 \end{pmatrix}, \qquad |11\rangle = \begin{pmatrix} 0 \\ 1 \end{pmatrix} \otimes \begin{pmatrix} 0 \\ 1 \end{pmatrix} = \begin{pmatrix} 0 \\ 0 \\ 0 \\ 1 \end{pmatrix} \tag{3}$$

and a general two-qubit state has the form

$$|\psi\rangle = \alpha|00\rangle + \beta|01\rangle + \gamma|10\rangle + \delta|11\rangle. \tag{4}$$

Multi-qubit states can be classified as either product states or entangled states. Product states can be written as tensor products of fewer qubit (subsystem) wave functions, for example

$$\frac{1}{\sqrt{2}}\big(|00\rangle + |01\rangle\big) = |0\rangle \otimes \frac{1}{\sqrt{2}}\big(|0\rangle + |1\rangle\big) \tag{5}$$

is one of the two-qubit states from Eq. (4), which is a product state. On the other hand

$$\frac{1}{\sqrt{2}}\big(|00\rangle + |11\rangle\big) \tag{6}$$

cannot be written as a tensor product of subsystem wave functions and thus is entangled. The entanglement is a very interesting property stemming from the foundation of quantum mechanics, which does not have a classical counterpart, and is a key ingredient in quantum computation and quantum information, e.g., in quantum teleportation [9] (more about entanglement is given in other chapters). Each of the computational basis states can represent one decimal number in its binary form, e.g. $|4\rangle = |100\rangle$ (we employ the notation that the rightmost qubit is the first one).

A quantum circuit is composed of quantum gates acting on qubits, which are usually initialized in a $|\text{zero}\rangle = |0\dots0\rangle$ state. Since the time evolution of quantum systems must be unitary, these gates are unitary operators. Quantum gates manipulate all components of a state vector, such as the one in Eq. (4), at the same time. This is so called quantum parallelism, which is however measurement limited.

Every multi-qubit unitary operation can be decomposed into single-, and entangling two-qubit gates [9]. Among the most important single qubit gates belong Pauli operators

$$X = \begin{pmatrix} 0 & 1 \\ 1 & 0 \end{pmatrix}, \quad Y = \begin{pmatrix} 0 & -i \\ i & 0 \end{pmatrix}, \quad Z = \begin{pmatrix} 1 & 0 \\ 0 & -1 \end{pmatrix}. \tag{7}$$

The Pauli matrices when exponentiated give rise to rotation operators about x, y and z axes, defined by the equations

$$R_x(\vartheta) = e^{-i\vartheta X/2} = \cos\frac{\vartheta}{2} I - i\sin\frac{\vartheta}{2} X = \begin{pmatrix} \cos\frac{\vartheta}{2} & -i\sin\frac{\vartheta}{2} \\ -i\sin\frac{\vartheta}{2} & \cos\frac{\vartheta}{2} \end{pmatrix}, \tag{8}$$

$$R_y(\vartheta) = e^{-i\vartheta Y/2} = \cos\frac{\vartheta}{2} I - i\sin\frac{\vartheta}{2} Y = \begin{pmatrix} \cos\frac{\vartheta}{2} & -\sin\frac{\vartheta}{2} \\ \sin\frac{\vartheta}{2} & \cos\frac{\vartheta}{2} \end{pmatrix}, \tag{9}$$

$$R_z(\vartheta) = e^{-i\vartheta Z/2} = \cos\frac{\vartheta}{2} I - i\sin\frac{\vartheta}{2} Z = \begin{pmatrix} e^{-i\frac{\vartheta}{2}} & 0 \\ 0 & e^{i\frac{\vartheta}{2}} \end{pmatrix}, \tag{10}$$

where I is the identity. Other very important single qubit gates include the Hadamard (denoted as Had not to confuse with the Hamiltonian) and T gates

$$\mathrm{Had} = \frac{1}{\sqrt{2}} \begin{pmatrix} 1 & 1 \\ 1 & -1 \end{pmatrix}, \quad \mathrm{T} = \begin{pmatrix} 1 & 0 \\ 0 & e^{i\pi/4} \end{pmatrix}. \tag{11}$$

The most common entangling two-qubit gate is the controlled-NOT (CNOT), which is a generalization of the classical XOR gate. Its action can be written as $|A, B\rangle \longrightarrow |A, B \oplus A\rangle$, where $\oplus$ is addition modulo two. The CNOT gate has the following circuit notation and matrix representation
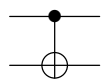
$$\begin{pmatrix} 1 & 0 & 0 & 0 \\ 0 & 1 & 0 & 0 \\ 0 & 0 & 0 & 1 \\ 0 & 0 & 1 & 0 \end{pmatrix}$$

and the action in the computational basis can be summarized as

$$|00\rangle \longrightarrow |00\rangle; \quad |01\rangle \longrightarrow |01\rangle; \quad |10\rangle \longrightarrow |11\rangle; \quad |11\rangle \longrightarrow |10\rangle. \tag{12}$$

One can see, that the NOT operation (X gate) is applied on the first qubit (rightmost in the ket, bottommost in the circuit), if the so called control qubit is in the state $|1\rangle$.

A final part of quantum circuits is a measurement that reveals some information. In quantum mechanics, a measurement is destructive, because it destroys superpositions. For example, when measuring the two-qubit state in Eq. (4) in the computational basis, the outcome will be one of the four possible states with the probability equal to the square of the absolute value of the expansion coefficient, e.g., the state $|00\rangle$ will be measured with probability $|\alpha|^2$.

wire carrying a qubit	$\lvert q \rangle$ ———————
measurement: projection onto $\lvert 0 \rangle$ and $\lvert 1 \rangle$	$\lvert q \rangle$ —[⟋]=
single-qubit unitary gate U	$\lvert q \rangle$ —[U]—
controlled-NOT operation	$\lvert q_2 \rangle$ ——•—— $\lvert q_1 \rangle$ —⊕—
controlled-U operation	$\lvert q_2 \rangle$ ——•—— $\lvert q_1 \rangle$ —[U]—
qubits ordering convention: $\lvert q_n \ldots q_2 q_1 \rangle$	$\lvert q_n \rangle$ ———————— $\vdots$ $\lvert q_2 \rangle$ ———————— $\lvert q_1 \rangle$ ————————

Fig. 2: *The quantum circuit model notation.*

Generally, having a register of qubits in the state $\lvert \psi \rangle$, we can measure some observable O, which is represented by a Hermitian matrix. One is usually interested in an average value over many measurements, i.e., the expectation value of O

$$\langle O \rangle = \langle \psi \lvert O \rvert \psi \rangle. \tag{13}$$

Measuring in the computational basis of ith qubit corresponds to the expectation value of the Pauli Z operator, $\langle \psi \lvert Z_i \rvert \psi \rangle$. This expectation value is in practice obtained by repeated measurement of qubit i (each time the state $\lvert \psi \rangle$ must be reinitialized) and averaging the outcomes of individual measurements ($+1$ for $\lvert 0 \rangle$ and -1 for $\lvert 1 \rangle$). As we will see in Sec. 4, strings of fermionic second quantized operators can be represented as strings of the Pauli operators. Therefore, in order to measure the expectation value of molecular Hamiltonians, we need also to measure in X and Y bases. These measurements can be realized by first applying single qubit rotations changing the basis, e.g., from X to Z and then measuring in the Z basis. One can easily verify that the Hadamard gate with the matrix representation in Eq. (11) transforms X eigenstates to Z eigenstates (and vice versa)

$$\frac{1}{\sqrt{2}} \begin{pmatrix} 1 & 1 \\ 1 & -1 \end{pmatrix} \cdot \frac{1}{\sqrt{2}} \begin{pmatrix} 1 \\ 1 \end{pmatrix} = \begin{pmatrix} 1 \\ 0 \end{pmatrix}, \tag{14}$$

$$\frac{1}{\sqrt{2}} \begin{pmatrix} 1 & 1 \\ 1 & -1 \end{pmatrix} \cdot \frac{1}{\sqrt{2}} \begin{pmatrix} 1 \\ -1 \end{pmatrix} = \begin{pmatrix} 0 \\ 1 \end{pmatrix}. \tag{15}$$

In Fig. 2, we summarize the quantum circuit model notation that is used throughout this chapter.
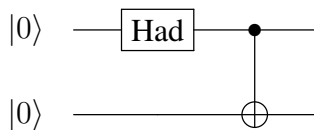
Fig. 3: *A quantum circuit which generates the Bell state* $\frac{1}{\sqrt{2}}\big(|00\rangle + |11\rangle\big)$.

As an example of a simple quantum circuit, we show in Fig. 3 the circuit, which generates the entangled state from Eq. (6) (the so called Bell state [9]). We employ the standard convention that time flows from left to right, i.e., first the Hadamard gate is applied on $|00\rangle$ forming

$$\frac{1}{\sqrt{2}}\big(|00\rangle + |10\rangle\big), \tag{16}$$

then the CNOT gate produces the final Bell state.

2.2 Quantum simulation

Quantum simulation can be either analog or digital. In case of analog simulators [10], a Hamiltonian of a studied system is mapped onto a tunable purpose-built quantum device (described by the same type of Hamiltonian), which then emulates the original system's dynamics. Any observable can be read out using suitable measurements. Analog simulators are very attractive as they are generally more robust to noise, which makes them suitable candidates for the near term quantum devices. However, in a long run, the lack of error correction is problematic for simulations of larger systems.

On the other hand, digital quantum simulation is realized by a quantum circuit (composed of single and two-qubit gates) implemented on an universal quantum computer. Digital quantum simulation can concern time evolution (dynamics) as well as computations of some static properties, such as the ground state energy.

The quantum algorithms for simulation of quantum dynamics were originally developed by Abrams and Lloyd [11, 12]. In order to time-evolve the studied system wave function on a register of qubits, one has to first map the initial system wave function (at time $t = 0$) onto the register, as well as map the system Hamiltonian to its qubit representation (H_q). The time evolution is then performed by the unitary propagator e^{-itH_q}, which is decomposed to elementary single and two-qubit gates. In quantum chemistry, we are interested in cases, when the system Hamiltonian contains polynomial number of terms (due to the two-body nature of molecular Hamiltonians)

$$H = \sum_j h_j, \tag{17}$$

which, however, mutually do not commute. The exponential of a Hamiltonian thus cannot be written as a product of the exponentials of individual h_j terms, but a numerical approximation must be used [11].

The first-order Trotter approximation [13] can be expressed as

$$e^{-itH} = e^{-it\sum_{j=1} h_j} = \left(\prod_{j=1} e^{-ih_j t/N}\right)^N + \mathcal{O}(t^2/N). \tag{18}$$

We would like to note that Trotterization is not the only possible way to simulate a Hamiltonian time evolution. Other approaches, which are however much more involved, will be briefly mentioned in Sec. 5.1 in the context of phase estimation algorithm. It has also been shown that time evolution can be simulated using variational algorithms [14]. Variational algorithms are discussed in Sec. 5.2.

As a simple example of quantum simulation, let us consider a spin chain model with an Ising Hamiltonian of the following form, which we adopted from [5]

$$H_{\text{Ising}} = \sum_{\langle i,j \rangle} J_{ij} Z_i Z_j + \sum_i B_i X_i, \tag{19}$$

where the first sum is over nearest-neighbor spins. In this spin case, the qubit representations of the wave function as well as the Hamiltonian are simple; $|0\rangle$ represents α spin, $|1\rangle$ represents β spin and the Hamiltonian in Eq. (19) has already a proper qubit form. After Trotterization, the Hamiltonian time evolution can be implemented by means of the terms

$$e^{-iJ_{ij}Z_i Z_j \delta t} \quad \text{and} \quad e^{-iB_i X_i \delta t}, \quad \text{where} \quad \delta t = t/N. \tag{20}$$

The second one corresponds to a rotation about x axis (Eq. (8)) applied on the ith qubit, $R_x^i(2B_i\delta t)$. The first term in Eq. (20) has a diagonal form in the computational basis with $e^{\pm iJ_{ij}\delta t}$ on the diagonal. The sign depends on the parity of the corresponding basis state and the exponential can be implemented with the following circuit [9]

$$ \tag{21}$$

where CNOTs assure the correct sign of the exponent according to the parity of the state and rotation about z axis is defined in Eq. (10).

In Fig. 4, we show a quantum circuit corresponding to the time evolution governed by the Ising Hamiltonian (Eq. (19)), which uses the first-order Trotter approximation [13]. The sequence of Hadamard gates in the beginning constitutes the state preparation and effectively aligns the spins along the x axis. The unitaries U_{m} change the basis before the measurement and their form depends on what exactly is measured (e.g. spin correlation functions) [12].

The original quantum algorithm for obtaining static properties of quantum systems by means of digital quantum simulation was developed by Abrams and Lloyd [15] and is based on the phase estimation algorithm [9]. We will discuss this approach in detail in the context of quantum chemistry and molecular Hamiltonians in Sec. 5.1.
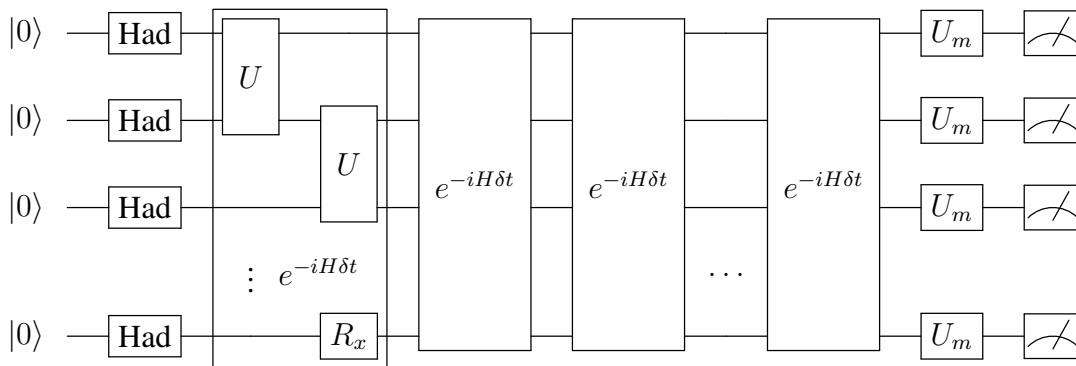
Fig. 4: *Scheme of a digital quantum simulation of the dynamics of a spin chain (Eq. (19)), which employs the first-order Trotter approximation. The two-qubit unitary gates correspond to $U_{ij} = CNOT^{i,j} R_z^j(2J_{ij}\delta t) CNOT^{i,j} R_x^i(2B_i\delta t)$.*

3 Quantum chemistry in a nutshell

We are predominantly interested in the electronic structure of molecules, whose Hamiltonians can be written (in atomic units) as

$$H = -\sum_i \frac{\nabla_i^2}{2} - \sum_I \frac{\nabla_I^2}{2M_I} - \sum_{i,I} \frac{Z_I}{|\mathbf{r}_i-\mathbf{R}_I|} + \frac{1}{2}\sum_{i\neq j} \frac{1}{|\mathbf{r}_i-\mathbf{r}_j|} + \frac{1}{2}\sum_{I\neq J} \frac{Z_I Z_J}{|\mathbf{R}_I-\mathbf{R}_J|}, \qquad (22)$$

where M_I, $\mathbf{R}_I$, and Z_I are the mass, position, and charge of the Ith nucleus and $\mathbf{r}_i$ is the position of ith electron. Taking into account that nuclei are more than 1000 times heavier than electrons, we can employ the Born-Oppenheimer approximation, which separates the electronic and nuclear parts of the Hamiltonian in Eq. (22) and solves them separately. Nuclei are then treated as classical point charges fixed at given positions in the electronic Hamiltonian

$$H_{\text{el.}} = -\sum_i \frac{\nabla_i^2}{2} + \frac{1}{2}\sum_{i\neq j} \frac{1}{|\mathbf{r}_i-\mathbf{r}_j|} - \sum_{i,I} \frac{Z_I}{|\mathbf{r}_i-\mathbf{R}_I|}. \qquad (23)$$

The Born-Oppenheimer approximation gives rise to the concept of the potential energy surfaces. Most of the quantum algorithms for chemical problems use this approximation, but there are exceptions. They comprise the first-quantized (Sec. 4.1) grid-based method [16] as well as the second-quantized (Sec. 4.2) nuclear and electron orbitals approach [17]. Both approaches treat nuclei and electrons on an equal footing.

3.1 Hartree-Fock method

The standard starting point of most of the electronic structure methods is the Hartree-Fock approximation. By using a wave function in the form of a single Slater determinant (see below) and applying the variational principle, it converts the N-electron problem in Eq. (23) to one-electron problems [18]. Electrons in the Hartree-Fock approximation are moving in an effective mean field of all the others. It is a so called mean-field approach.

As was mentioned above, the essence of the Hartree-Fock approximation is a wave function in the form of a single Slater determinant (or spin-adapted combination of few of them in case of open-shell problems)

$$\Phi(\mathbf{x}_1, \mathbf{x}_2, \ldots, \mathbf{x}_N) = \frac{1}{\sqrt{N!}} \begin{vmatrix} \chi_1(\mathbf{x}_1) & \chi_1(\mathbf{x}_2) & \ldots & \chi_1(\mathbf{x}_N) \\ \chi_2(\mathbf{x}_1) & \chi_2(\mathbf{x}_2) & \ldots & \chi_2(\mathbf{x}_N) \\ \vdots & \vdots & \vdots & \vdots \\ \chi_N(\mathbf{x}_1) & \chi_N(\mathbf{x}_2) & \ldots & \chi_N(\mathbf{x}_N) \end{vmatrix} \equiv |\chi_1 \chi_2 \ldots \chi_N\rangle. \qquad (24)$$

Here $\mathbf{x}_i$ are composite spatial and spin coordinates of the ith electron, $\mathbf{x}_i = (\mathbf{r}_i, \sigma_i)$ and χ_j are one-electron wave functions, molecular spin-orbitals, which are obtained by solution of the Fock operator eigenvalue problem

$$f(\mathbf{x}_1)\chi_i(\mathbf{x}_1) = \varepsilon_i \chi_i(\mathbf{x}_1). \qquad (25)$$

The Fock operator $f(\mathbf{x}_1)$ has the form [18]

$$f(\mathbf{x}_1) = -\frac{\nabla_1^2}{2} - \sum_I \frac{Z_I}{|\mathbf{r}_1 - \mathbf{R}_I|} + v^{\text{HF}}(\mathbf{x}_1), \qquad (26)$$

where $v^{\text{HF}}(\mathbf{x}_1)$ represents the operator of a mean field potential of the remaining electrons

$$v^{\text{HF}}(\mathbf{x}_1) = \sum_i \int \chi_i^*(\mathbf{x}_2) \frac{1}{|\mathbf{r}_1 - \mathbf{r}_2|} (1 - P_{12}) \chi_i(\mathbf{x}_2) \mathrm{d}\mathbf{x}_2, \qquad (27)$$

and the permutation operator P_{12} permutes indices of both electrons. The eigenvalues ε_i in Eq. (25) are spin-orbital energies.

The Slater determinant form of a wave function, Eq. (24), correctly accounts for the exchange symmetry stemming from the fermionic nature of electrons. In fact, swapping any two electrons is equivalent to interchanging two columns of the determinant, which changes the sign of the wave function.

The Hartree-Fock equations, Eq. (25), are in fact nonlinear integro-differential equations, which are usually solved numerically via expansion of molecular orbitals[3] in an atomic orbital basis

$$\psi_i(\mathbf{r}) = \sum_\mu C_{\mu i} \varphi_\mu(\mathbf{r}). \qquad (28)$$

The expansion coefficients $C_{\mu i}$ then represent variational parameters optimized during the self-consistent-field (SCF) procedure [18]. The most common atomic orbital basis functions $\varphi_\mu(\mathbf{r})$ are Gaussian-type orbitals (GTOs). GTOs obey the usual radial-angular decomposition

$$\varphi(\mathbf{r}) = R_{nl}(r) Y_{lm}(\vartheta, \varphi), \qquad (29)$$

---

[3]Since the non-relativistic electronic Hamiltonian (Eq. (23)) does not contain spin-dependent operators, the spin can be effectively integrated out, transforming the original problem of molecular spin-orbitals to the problem of molecular orbitals.

with $Y_{lm}(\vartheta, \varphi)$ being spherical harmonic functions and the radial part is of the form

$$R_{nl}^{\text{GTO}}(r) \propto (\sqrt{\alpha_{nl}}\, r)^l e^{-\alpha_{nl} r^2}, \tag{30}$$

where l denotes the angular momentum quantum number of the orbital and α_{nl} is a fitting parameter. Gaussian-type orbitals do not form as compact basis sets as Slater-type orbitals (STOs), which have the correctly behaving radial part of the hydrogen atom solution

$$R_n^{\text{STO}}(r) \propto (\zeta r)^{n-1} e^{-\zeta r}, \tag{31}$$

however, two-electron integral evaluation with GTOs is much easier. For this reason, the most common basis sets used in quantum chemistry are contracted GTOs. In this case, each basis function is a fixed linear combination (contraction) of Gaussian functions (so called primitives). The contraction coefficients as well as exponents of Gaussian functions are pre-optimized for standard basis sets [19]. Regarding the flexibility of basis sets, the minimal basis (e.g. STO-3G) contains all orbitals involved in the Hartree-Fock Slater determinant (occupied ones) plus orbitals of the same/similar energy (e.g. all orbitals of a given open shell). For atoms such as lithium, basis functions of p type are also added to the $1s$ and $2s$ orbitals, because lithium also has a $1s2p$ bound state. The lithium minimal basis thus contains $\{1s, 2s, 2p_x, 2p_y, 2p_z\}$.

Since the valence electrons are the most important ones for chemistry (they participate in bonding), it is not surprising that valence orbitals are commonly represented by more than one basis function. These basis sets are denoted as split-valence and according to the number of basis functions per valence orbital are called valence double, triple, quadruple-ζ, etc. basis sets. Additional polarization functions (with higher angular momentum) or diffuse functions (with small exponents) can further increase the flexibility of GTO basis sets.

In spite of the fact that GTOs have been used in mainstream quantum chemistry for decades, it turns out that they may not be the best basis sets for use in connection with quantum algorithms. Their problem lies in a number of terms in a second-quantized form of a Hamiltonian (see Sec. 3.3), which scales as $\mathcal{O}(M^4)$, where M is the basis set size. The number of terms in a Hamiltonian largely influences the cost of quantum algorithms, as will be discussed below. Babbush *et al.* [20] pointed out this problem and suggested the use of the plane wave basis and its dual representation. The plane wave basis functions have the form

$$\varphi_{\mathbf{G}}^{\mathbf{k}}(\mathbf{r}) = \frac{1}{\sqrt{\Omega}} e^{i(\mathbf{k}+\mathbf{G})\mathbf{r}}, \tag{32}$$

where Ω is the computational cell volume, $\mathbf{k}$ the wave vector, and $\mathbf{G}$ denote the reciprocal lattice vectors. The Fourier transform of the complete plane wave basis would lead to a basis of delta functions (a grid), thus by applying the discrete Fourier transform on an incomplete plane wave basis, one obtains a so called plane wave dual basis [20], which resembles a smooth approximation to a grid. Direct use of the plane wave basis leads to a reduction of the Hamiltonian terms from $\mathcal{O}(M^4)$ to $\mathcal{O}(M^3)$ (due to the momentum conservation). The plane wave dual basis which diagonalizes the two-body potential operator reduces the number of Hamiltonian terms to $\mathcal{O}(M^2)$ [20]. The plane wave basis sets have been traditionally used for density functional

theory (DFT) calculations of periodic systems. They can also be used for isolated molecules, however, for a given accuracy about hundred times more plane wave basis functions than GTOs are necessary.

The basis set methods exploit some suitable basis in order to make the wave function expansion as compact as possible (or decrease the number of terms in the Hamiltonian, or ideally both). Alternatively, one can employ grid based methods. In this case, the wave function is expanded on a discretized spatial grid (basis of delta functions at given positions $\{|r\rangle\}$) and has a form

$$|\Psi\rangle = \sum_{\mathbf{x}_1...\mathbf{x}_N} \psi(\mathbf{x}_1, \mathbf{x}_2, \ldots \mathbf{x}_N) \mathcal{A}(|\mathbf{x}_1, \mathbf{x}_2, \ldots \mathbf{x}_N\rangle), \tag{33}$$

where $|\mathbf{x}_i\rangle$ is the composite spatial and spin coordinate ($|\mathbf{r}_i\rangle|\sigma_i\rangle$) of the ith electron and $\mathcal{A}$ is the operator assuring proper antisymmetrization of the wave function. Classically, such approaches (without further approximations) are exponentially costly, because they naturally face the original problem of exponentially large Hilbert space. If each of the $3N$ coordinate axis is discretized to P equidistant points, then the number of expansion coefficients $\psi(\mathbf{x}_1, \mathbf{x}_2, \ldots \mathbf{x}_N)$ scales as $P^{3N} \times 2^N$. On the other hand, the grid-based quantum simulations can be *efficient*, as will be briefly discussed in Sec. 4.1.

3.2   Correlation energy

The Hartree-Fock method is derived based on the approximation of the N-electron wave function in the form of a single Slater determinant (or their spin-adapted combination) as shown in Eq. (24). Even if we solve the Hartree-Fock equations (Eq. (25)) exactly (in the limit of the complete basis set), we will certainly not get the exact energy, because the movement of electrons is not properly correlated at a single determinant level (e.g. electrons with opposite spins are allowed to be at the same place).

The exact wave function, for a given one-particle basis, which were discussed above, can be written as

$$|\Psi\rangle_{\text{FCI}} = c|\Phi\rangle + \sum_{ia} c_i^a |\Phi_i^a\rangle + \sum_{\substack{a<b \\ i<j}} c_{ij}^{ab} |\Phi_{ij}^{ab}\rangle + \cdots, \tag{34}$$

where $|\Phi\rangle$ is the Hartree-Fock Slater determinant (Eq. (24)), $i, j, \ldots$ are indices of occupied orbitals, $a, b, \ldots$ are indices of virtual orbitals (at the Hartree-Fock level), and $\Phi_{ij\ldots}^{ab\ldots}$ denote excited Slater determinants with respect to the Hartree-Fock one (singly excited $i \to a$, doubly excited $ij \to ab$, ..., up to N-electron excited). This exact wave function form corresponds to the full configuration interaction (FCI) method. Since the number of Slater determinants in the FCI expansion (Eq. (34)) scales exponentially with the number of electrons (see Fig. 1), only the smallest molecules can be treated by FCI (up to approx. 20 electrons in 20 orbitals).

The correlation energy is defined as the difference between the FCI energy in the limit of a complete basis set and the Hartree-Fock energy in the same limit

$$\Delta E_{\text{corr}} = E^{\text{FCI-lim.}} - E^{\text{HF-lim.}}. \tag{35}$$

In spite of the fact that the correlation energy is only about 1 % of the Hartree-Fock energy, it is orders of magnitude larger than reaction or activation enthalpies of chemical reactions even for small molecules and its, at least approximative, treatment is absolutely essential for chemically relevant results. The correlation energy is calculated by post-Hartree-Fock methods (we will briefly mention two of them, the configuration interaction method in Sec. 3.3.1 and the coupled cluster approach in Sec. 3.3.2). We can formally express the transition from the reference (Hartree-Fock) wave function to the exact one by means of the wave operator Ω

$$|\Psi\rangle = \Omega|\Phi_{\mathrm{HF}}\rangle. \tag{36}$$

A widely used accuracy threshold of 1 kcal/mol ($1.6 \cdot 10^{-3}$ Hartree) is known as "chemical accuracy". If the energy difference between the transition state of a chemical reaction and the reactant ($\Delta E^{\dagger}$) is given within this accuracy threshold, then the reaction rate at room temperature can be predicted to within an order of magnitude with the Eyring equation

$$v \propto e^{-\Delta E^{\dagger}/k_B T}, \tag{37}$$

where T denotes the temperature and k_B is the Boltzmann constant. The concept of the chemical accuracy is also widely used in the quantum computational chemistry community [5]. Usually, the experimental realizations of quantum algorithms for chemistry (or their simulations) are compared against the chemical accuracy [5,6].

As was mentioned above, electrons are not properly correlated at the Hartree-Fock level. Very often, the correlation effects (and their contributions to the correlation energy) are divided into dynamic (or weak) electron correlation and static (or strong) electron correlation. The former one is usually a small correction to the wave function (the Hartree-Fock determinant is by far the most dominant one) and is a result of improper treatment of Coulomb repulsion in the single-determinant Hartree-Fock approach. The dynamic electron correlation can be accounted for by an expansion into a large number of Slater determinants systematically formed from the Hartree-Fock reference (single excitations, single and double excitations, etc.), e.g., via the configuration interaction or coupled cluster methods (see Sec. 3.3), or to a large extent also by means of density functional theory. These methods are called single reference and they work very well, when the wave function can be qualitatively described by a single Slater determinant. DFT has a favorable scaling and can treat hundreds of atoms. If spectroscopic accuracy is desired, coupled cluster theory is often the first choice with CCSD(T) being the "gold standard" of quantum chemistry [21].

The static correlation is a result of quasidegeneracy of molecular orbitals and manifests itself by several equally dominant Slater determinants in a wave function expansion. Many important chemical problems fall into this category, e.g. homolytic bond breaking/formation, open-shell and excited electronic states, transition-metal complexes, and transition states of chemical reactions [22]. They are called multireference or strongly correlated. When the manifold of quasidenerate orbitals is small and can be treated by FCI, the active space methods (e.g. complete active space self consistent field, CASSCF) with perturbative dynamic electron correlation extensions can be used. However, when tens of orbitals are strongly correlated, the situation is
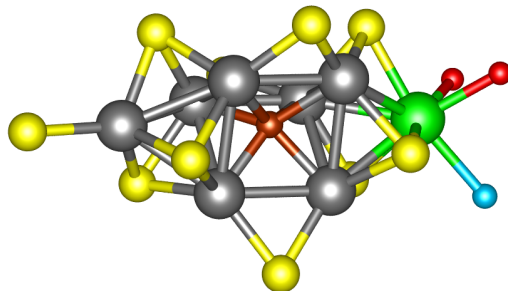
Fig. 5: *Structure of the FeMoco cluster. For clarity, only the atoms of the ligands which are directly bonded to Fe and Mo atoms are displayed. Atom colors: nitrogen - blue, sulphur - yellow, oxygen - red, carbon - brown, iron - grey, molybdenum - green.*

much more complicated. The classical computational methods like tensor networks with the density matrix renormalization group (DMRG), different flavors of quantum Monte Carlo, or e.g., selected configuration interaction approaches, which can treat larger active spaces than exact diagonalization allows, in fact have their own limitations. These are the situations, where quantum algorithms are believed to become a game changer [6].

We have already mentioned in the introduction that catalysts or high temperature superconductors belong to the class of very important strongly correlated problems. As a concrete example, let us mention the electronic structure problem of the Mo-dependent nitrogenase active site (FeMo cofactor, FeMoco), whose structure is depicted in Fig. 5. It has been suggested by Reiher *et al.* [23] as a prominent candidate for quantum simulation algorithms. Enzyme nitrogenase is transforming N_2 into two NH_3 molecules under ambient conditions and understanding of this very complex process, whose mechanism is still not known, is of very high scientific and economic importance. In fact, 2 % of the annual energy production is consumed in the energetically demanding industrial Haber-Bosch synthesis of ammonia. The electronic structure problem of FeMoco is one of the most challenging problems of current computational chemistry.

3.3 Second quantization

Quantum mechanics can be formulated either in the first, or in the second quantization. In the former case, operators are assigned to variables like position or momentum. In the later one, fields rather than variables are quantized. The formalism of second quantization is widely used also in quantum chemistry [18]. Using this formalism, we can transform properties of determinants into algebraic properties of creation and annihilation operators. We restrict ourselves to orthonormal bases of spin orbitals.

The creation operator $a_p^\dagger$ creates an electron in the pth spin orbital. On the contrary, the annihilation operator a_q destroys an electron in the qth spin orbital. These operators obey fermionic anti-commutation rules

$$\{a_p,\, a_q^\dagger\} \;=\; a_p a_q^\dagger + a_q^\dagger a_p = \delta_{pq}, \tag{38}$$

$$\{a_p,\, a_q\} \;=\; \{a_p^\dagger,\, a_q^\dagger\} = 0, \tag{39}$$

which ensure proper anti-symmetry of a wave function and also satisfy the Pauli exclusion principle (if $p = q$, then $a_p^\dagger a_p^\dagger = 0$).

Slater determinants are represented in the occupation basis

$$\Phi(\mathbf{x}_1, \mathbf{x}_2, \ldots, \mathbf{x}_N) = |o_1, \ldots, o_p, \ldots, o_M\rangle, \tag{40}$$

where o_p is equal to 1, when χ_p is occupied, or 0, when it is unoccupied. In other words, kets in the occupation basis representation are binary strings with the length of the number of spin orbitals, in which ones define which spin orbitals are occupied. In order to demonstrate the action of second-quantized operators on determinants, let us take a simple example of the hydrogen molecule (H_2) in a minimal basis (we will use this example also further). Each of the two hydrogen atoms is described with one $1s$ atomic orbital, which are combined into the two molecular orbitals: bonding (denoted as *gerade*, 'g'), which is lower in energy, and antibonding (denoted as *ungerade*, 'u'), which is higher in energy. If we order orbitals in occupation binary strings according to the energy from the left to the right (α spin preceding β), the H_2 determinants in a minimal basis are represented as $|o_{g\uparrow} o_{g\downarrow} o_{u\uparrow} o_{u\downarrow}\rangle$. The Hartree-Fock state is given by

$$\Phi_{\text{HF}} = |1100\rangle = a_{g\uparrow}^\dagger a_{g\downarrow}^\dagger |\rangle, \tag{41}$$

where $|\rangle$ denotes the normalized vacuum state, which does not contain any electrons and thus $a_p|\rangle = 0$. If we now apply, e.g., $a_{g\downarrow}$ on Φ_{HF}, we have

$$a_{g\downarrow}|1100\rangle = a_{g\downarrow} a_{g\uparrow}^\dagger a_{g\downarrow}^\dagger |\rangle = -a_{g\uparrow}^\dagger a_{g\downarrow} a_{g\downarrow}^\dagger |\rangle = -a_{g\uparrow}^\dagger (1 - a_{g\downarrow}^\dagger a_{g\downarrow})|\rangle = -a_{g\uparrow}^\dagger |\rangle = -|1000\rangle \tag{42}$$

where we have used Eq. (38) twice and the aforementioned property of $|\rangle$. The minus sign in Eq. (42) is the result of fermionic exchange anti-symmetry. In fact, the action of creation and annihilation operators on general determinants can be summarized as

$$a_p|o_1, \ldots, o_p, \ldots, o_M\rangle \;=\; \delta_{o_p,1}(-1)^{\sum_{i=1}^{p-1} o_i}|o_1, \ldots, o_p \oplus 1, \ldots, o_M\rangle, \tag{43}$$

$$a_p^\dagger|o_1, \ldots, o_p, \ldots, o_M\rangle \;=\; \delta_{o_p,0}(-1)^{\sum_{i=1}^{p-1} o_i}|o_1, \ldots, o_p \oplus 1, \ldots, o_M\rangle, \tag{44}$$

where $\oplus$ stands for addition modulo 2 ($0 \oplus 1 = 1$, $1 \oplus 1 = 0$).

Slater determinants excited with respect to the Hartree-Fock state as used in Eq. (34) can be written as

$$|\Phi_i^a\rangle = a_a^\dagger a_i|\Phi\rangle, \tag{45}$$

$$|\Phi_{ij}^{ab}\rangle = a_a^\dagger a_b^\dagger a_j a_i|\Phi\rangle, \quad \text{etc.} \tag{46}$$

As mentioned above, in second quantization, the proper anti-symmetry of a wave function is maintained by properties of creation and annihilation operators applied on it. On the other hand in first quantization, the operators applied on a wave function retain its anti-symmetry, which must be explicitly created during an initialization (see Sec. 4.1).

An arbitrary one-electron operator O_1, which can be written as a sum of one-electron contributions $\sum_i^N o_1(\mathbf{x}_i)$, has the following second-quantized representation [18]

$$O_1 = \sum_{pq} \langle p|o_1|q \rangle \, a_p^\dagger a_q, \tag{47}$$

where $\langle p|o_1|q \rangle$ denote the one-electron integrals

$$\langle p|o_1|q \rangle \equiv \int \chi_p(\mathbf{x}_1)^* o_1(\mathbf{x}_1) \chi_q(\mathbf{x}_1) \, d\mathbf{x}_1. \tag{48}$$

Analogously a two-electron operator O_2, which is expressed as a sum of two-electron contributions $\sum_{i<j}^N o_2(\mathbf{x}_i, \mathbf{x}_j)$, can be written as [18]

$$O_2 = \frac{1}{2} \sum_{pqrs} \langle pq| \, o_2|rs \rangle a_p^\dagger a_q^\dagger a_s a_r, \tag{49}$$

with

$$\langle pq|o_2|rs \rangle \equiv \int \chi_p(\mathbf{x}_1)^* \chi_q(\mathbf{x}_2)^* o_2(\mathbf{x}_1, \mathbf{x}_2) \chi_r(\mathbf{x}_1) \chi_s(\mathbf{x}_2) \, d\mathbf{x}_1 d\mathbf{x}_2. \tag{50}$$

One can easily verify that such definitions satisfy the general Slater-Condon rules for matrix elements [18]. Based on these definitions, we can write the electronic Hamiltonian from Eq. (23) in the second-quantized form as

$$H = \sum_{pq} h_{pq} \, a_p^\dagger a_q + \frac{1}{2} \sum_{pqrs} \langle pq|rs \rangle \, a_p^\dagger a_q^\dagger a_s a_r, \tag{51}$$

where the one and two-electron integrals have the form

$$h_{pq} = \int \chi_p(\mathbf{x}_1)^* \left(-\frac{\nabla^2}{2} - \sum_I \frac{Z_I}{|\mathbf{r}_1 - \mathbf{R}_I|} \right) \chi_q(\mathbf{x}_1) \, d\mathbf{x}_1, \tag{52}$$

$$\langle pq|rs \rangle = \int \frac{\chi_p(\mathbf{x}_1)^* \chi_q(\mathbf{x}_2)^* \chi_r(\mathbf{x}_1) \chi_s(\mathbf{x}_2)}{|\mathbf{r}_1 - \mathbf{r}_2|} \, d\mathbf{x}_1 d\mathbf{x}_2 \,. \tag{53}$$

One can see in Eq. (51) that the Hamiltonian contains up to M^4 terms (depending on the basis functions used) and these terms contain only up to four second-quantized operators (Coulomb interaction is two-body).

The formalism of second-quantization is commonly used in the derivation of computational methods. In what follows, we will very briefly mention two approaches, which are important for further discussion, namely the configuration interaction (CI) and coupled cluster (CC) methods.

3.3.1 Configuration interaction method

The configuration interaction is a variational method, which unlike the Hartree-Fock approach is not restricted to a single Slater determinant, but the wave function has the form of a linear

combination of the ground and excited Slater determinants. The wave function of the full configuration interaction (FCI) was already shown in Eq. (34). The wave operator, Eq. (36), can be written as

$$\Omega_{\mathrm{CI}} = c + \sum_\alpha C_\alpha, \tag{54}$$

where

$$C_1 = \sum_{ia} c_i^a a_a^\dagger a_i, \tag{55}$$

$$C_2 = \sum_{\substack{a<b \\ i<j}} c_{ij}^{ab} a_a^\dagger a_b^\dagger a_j a_i, \tag{56}$$
$$\vdots$$

with c, $c_{ij\ldots}^{ab\ldots}$ being the variational parameters. The FCI wave function contains all possible Slater determinants formed by placing N_α and N_β electrons in $M/2$ orbitals and is exact within a given orbital basis. However, its computational cost scales exponentially with the system size. Therefore, the CI method is typically restricted to including only certain excitations, most commonly single excitations (C_1, denoted as CIS) or single and double excitations (C_1, C_2, denoted as CISD).

The consequences of the linear form of the wave operator (Eq. (54)) are slow convergence to the FCI with increasing excitation rank as well as incorrect scaling of the energy with the system size (truncated CI is not size-extensive).

3.3.2   Coupled cluster method

The aforementioned limitations of the linear CI expansion are avoided in the coupled cluster (CC) theory. The CC wave operator has an exponential form

$$\Omega_{\mathrm{CC}} = e^T, \tag{57}$$

where T is the so called cluster operator

$$T = \sum_\alpha T_\alpha \tag{58}$$

and for T_α, it holds

$$T_1 = \sum_{ia} t_i^a a_a^\dagger a_i, \tag{59}$$

$$T_2 = \sum_{\substack{a<b \\ i<j}} t_{ij}^{ab} a_a^\dagger a_b^\dagger a_j a_i, \tag{60}$$
$$\vdots$$

where t parameters are CC amplitudes. Similarly to CI, the CC method is normally truncated to only certain excitations, e.g. single and double excitations, CCSD. The CCSD(T) method with

perturbative triple excitations and $\mathcal{O}(M^7)$ scaling is considered the "gold standard" of quantum chemistry [21].

The standard CC theory is unlike CI not variational, because direct application of the Rayleigh-Ritz variational principle on the wave function from Eq. (57) would lead to an infinite commutator expansion.[4] Instead, a projection technique is employed, which leads to closed explicit algebraic equations for the CC amplitudes, the so called amplitude equations.

The starting point in the derivation of the amplitude equations is the Schrödinger equation written using the CC wave function

$$H|\Psi\rangle = E|\Psi\rangle = Ee^T|\Phi_{\text{HF}}\rangle. \tag{61}$$

If we multiply the above Schrödinger equation on the left by e^{-T} and then project on Φ_{HF}, we get the CC energy formula

$$\langle\Phi_{\text{HF}}|e^{-T}He^T|\Phi_{\text{HF}}\rangle = E\langle\Phi_{\text{HF}}|\Phi_{\text{HF}}\rangle = E. \tag{62}$$

If we project onto the entire set of up to m-tuply excited determinants Φ^* (Φ_i^a, Φ_{ij}^{ab}, etc.), where m is the highest excitation rank in T, we get the amplitude equations mentioned above

$$\langle\Phi^*|e^{-T}He^T|\Phi_{\text{HF}}\rangle = E\langle\Phi^*|\Phi_{\text{HF}}\rangle = 0. \tag{63}$$

The unitary coupled cluster (UCC) approach employs the following unitary form of the wave operator

$$\Omega_{\text{UCC}} = e^{T-T^\dagger}. \tag{64}$$

The UCC method is superior to the standard CC [24], however for the same reason as the variational coupled cluster approach, it cannot be implemented efficiently on a classical computer. On the other hand, as we will discuss in Sec. 5.2, on a quantum computer the unitary ansatz is clearly advantageous as the wave function parametrization then straightforwardly and efficiently translates to a (unitary) quantum circuit.

4 Quantum chemistry to quantum computing mappings

In this section, we will discuss methods for encoding fermionic problems into qubits in both first and second quantization. In order to keep the text self-contained, we will mention in some detail also the most widely employed Jordan-Wigner mapping (Sec. 4.2), which is also discussed in a different chapter.

---

[4]The problem lies in the fact that a variational approach requires computation of $e^{T^\dagger}He^T$, which when employing the Baker-Campbell-Hausdorff formula does not produce a finite commutator expansion, because $T^\dagger$ contains de-excitations.

4.1   First quantized methods

First quantized methods can be grid based or employ the single-particle basis. We will follow the presentation given in the fantastic pedagogical review [5] and adopt some illustrative examples from there.

Let us start with grid based methods. In this case, the wave function is expanded on a discretized spatial grid and has the form shown in Eq. (33). Classically, it is not possible to store all the $P^{3N} \times 2^N$ complex amplitudes for larger systems, where P is the number of equidistant points in each axis. However, it can be done efficiently on a quantum computer. If P is expressed as power of 2, $P = 2^m$, then the number of complex amplitudes is equal to $P^{3N} \times 2^N = 2^{(3m+1)N}$. Taking into account properties of composite quantum systems discussed in Sec. 2.1, it is clear that $(3m+1)N$ qubits can store the wave function from Eq. (33).

As a simple example, we consider two spinless electrons on a four-point one-dimensional grid. Four points of a grid can be represented using 2 qubits: $|0\rangle \equiv |00\rangle$, $|1\rangle \equiv |01\rangle$, $|2\rangle \equiv |10\rangle$, and $|3\rangle \equiv |11\rangle$. As in [5], we distinguish two types of wave functions denoted as 'n' and 'u' shaped (according to the shape of amplitudes distribution). They have the form

$$|\varphi_{\mathrm{n}}\rangle = \frac{1}{\sqrt{6}}|0\rangle + \frac{1}{\sqrt{3}}|1\rangle + \frac{1}{\sqrt{3}}|2\rangle + \frac{1}{\sqrt{6}}|3\rangle, \tag{65}$$

$$|\varphi_{\mathrm{u}}\rangle = \frac{1}{\sqrt{3}}|0\rangle + \frac{1}{\sqrt{6}}|1\rangle + \frac{1}{\sqrt{6}}|2\rangle + \frac{1}{\sqrt{3}}|3\rangle. \tag{66}$$

In order to properly account for the fermionic exchange symmetry, one has to initially prepare the two-electron anti-symmetric wave function, such as

$$
\begin{aligned}
|\varPhi\rangle &= \frac{1}{\sqrt{2}}\Big(|\varphi_{\mathrm{n}}\rangle_1|\varphi_{\mathrm{u}}\rangle_2 - |\varphi_{\mathrm{u}}\rangle_1|\varphi_{\mathrm{n}}\rangle_2\Big) \\
&= \frac{1}{6\sqrt{2}}\Big(|1\rangle_1|0\rangle_2 - |0\rangle_1|1\rangle_2 + |1\rangle_1|3\rangle_2 - |3\rangle_1|1\rangle_2 + |2\rangle_1|0\rangle_2 - |0\rangle_1|2\rangle_2 + |2\rangle_1|3\rangle_2 - |3\rangle_1|2\rangle_2\Big),
\end{aligned}
\tag{67}
$$

where ket subscripts label the electrons. The wave function is then maintained anti-symmetric during the time evolution. We have already mentioned the Trotterized time evolution in Sec. 2.2 and will comment on other approaches in Sec. 5.1.

Grid-based approaches have certain advantages, but also certain disadvantages. Regarding the advantages, they achieve a good scaling and it is easy to generalize them for equal treatment of nuclei and electrons on a grid, thus avoiding the Born-Oppenheimer approximation. On the other hand, they require a lot more qubits (to represent a grid) than basis set approaches, which makes them unsuitable for near-term devices.

The original first-quantized basis set based algorithm for quantum simulation was developed by Abrams and Lloyd [12]. It uses $N\lceil\log_2 M\rceil$ qubits to represent N electrons in M basis functions. For each of the electrons, $\lceil\log_2 M\rceil$ qubits are necessary to assign a basis function, they are ordered from $|0\ldots00\rangle$ to $|1\ldots11\rangle$. The product of N-electron wave function then has to be antisymmetrized. The original approach [12] requires $\mathcal{O}(N^2\log_2^2 M)$ gates and also $\mathcal{O}(N\log_2 M)$ ancilla qubits.

As an illustrative example, we adopt the H_2 molecule in a minimal basis from Sec. 3.3 and label the molecular spin orbitals as $|g_\uparrow\rangle = |00\rangle = |0\rangle$, $|g_\downarrow\rangle = |01\rangle = |1\rangle$, $|u_\uparrow\rangle = |10\rangle = |2\rangle$, and $|u_\downarrow\rangle = |11\rangle = |3\rangle$. The simple product of one electron in the $|g_\uparrow\rangle$ spin orbital and the other in $|g_\downarrow\rangle$ representing the Hartree-Fock state is clearly not anti-symmetric. The properly anti-symmetrized Hartree-Fock state looks like

$$|\varPhi_{\text{HF}}\rangle = \frac{1}{\sqrt{2}}\big(|0\rangle_1|1\rangle_2 - |1\rangle_1|0\rangle_2\big). \tag{68}$$

The exact ground state wave function of the H_2 molecule in a minimal basis can be written as a linear combination of only two Slater determinants (we use the compact determinant notation from Eq. (24))

$$|\varPsi\rangle = \alpha|g_\uparrow g_\downarrow\rangle + \beta|u_\uparrow u_\downarrow\rangle = \frac{\alpha}{\sqrt{2}}\big(|0\rangle_1|1\rangle_2 - |1\rangle_1|0\rangle_2\big) + \frac{\beta}{\sqrt{2}}\big(|2\rangle_1|3\rangle_2 - |3\rangle_1|2\rangle_2\big), \tag{69}$$

because the remaining two fulfilling the $s_z = 0$ $\big(|g_\uparrow u_\downarrow\rangle, |g_\downarrow u_\uparrow\rangle\big)$ have different spatial symmetry ("ungerade") and thus does not contribute to the ground state wave function.

The Hamiltonian can be obtained by projection onto the single-particle basis

$$H = \sum_{i=1}^{N}\sum_{p,q=1}^{M} h_{pq}|\chi_p\rangle_i\langle\chi_q|_i + \frac{1}{2}\sum_{i\neq j}^{N}\sum_{p,q,r,s}^{M}\langle pq|rs\rangle|\chi_p\rangle_i|\chi_q\rangle_j\langle\chi_s|_j\langle\chi_r|_i, \tag{70}$$

where one and two-electron integrals h_{qp} and $\langle pq|qs\rangle$ were already defined in Eqs. (52) and (53). Individual operators from Eq. (70) can be straightforwardly expressed by means of the Pauli operators, Eq. (7), leading to the total number of $\mathcal{O}(N^2 M^6)$ Pauli terms, which are up to $2\log_2 M$-local [5]. The Hamiltonian can then be used to time evolve the anti-symmetrized wave function [12]. We will discuss the time evolution, which is a key part in many quantum simulation algorithms, in more detail in Sec. 5.1.

4.2 Second quantized methods

In this subsection, we will describe how to express the creation and annihilation operators of indistinguishable electrons in terms of the Pauli operators acting on distinguishable qubits, which can be achieved in multiple ways.

In case of the Jordan-Wigner (JW) mapping [25], qubit states encode the occupation vector (Eq. (40))

$$|o_1 \ldots o_M\rangle \rightarrow |q_M \ldots q_1\rangle, \qquad q_p = o_{M-p+1} \in \{0, 1\}. \tag{71}$$

Since we employ the standard conventions used in quantum chemistry and quantum computing communities, i.e., orbitals in occupation vectors are ordered from the left [18] and qubits in kets are ordered from the right [9], in what follows, we will use the primed indices for qubit labels with a simple conversion

$$p' = M - p + 1. \tag{72}$$

The second-quantized operators can be expressed as

$$a_p^\dagger = \left(\bigotimes_{j=1}^{p-1} Z_{j'}\right) \otimes Q_{p'}^\dagger, \quad a_p = \left(\bigotimes_{j=1}^{p-1} Z_{j'}\right) \otimes Q_{p'}, \tag{73}$$

where $Q = |0\rangle\langle 1| = (X+iY)/2$ and $Q^\dagger = |1\rangle\langle 0| = (X-iY)/2$. The strings of Pauli Z operators ensure the right phase factor / "parity of the state" as summarized in Eqs. (43) and (44), Q and $Q^\dagger$ then decrease or increase the occupation of a given spin orbital. One can easily verify that such a representation of the second quantized operators satisfies their anti-commutation relations (Eq. (38)).

The electronic Hamiltonian, Eq. (51), can be rewritten using strings of Pauli operators

$$H = \sum_j h_j P_j = \sum_j h_j \prod_i \sigma_{i'}^j, \tag{74}$$

where σ_i^j stands for one of the Pauli operators (X, Y, Z) or the identity acting on i^{th} qubit, the sum over j runs over all one and two-electron terms and h_j formally represent one and two-electron integrals. Finally the exponentials of these strings, which are required by some time evolution algorithms, can be build up from single qubit gates and CNOTs [9], similarly to the time evolution of the simple Ising model presented in Sec. 2.2. We will demonstrate this approach on the one-electron part of the non-relativistic (real) Hamiltonian

$$H_1 = \sum_{pq} h_{pq} a_p^\dagger a_q = \sum_p h_{pp} a_p^\dagger a_p + \sum_{p<q} \left(h_{pq} a_p^\dagger a_q + h_{qp} a_q^\dagger a_p\right). \tag{75}$$

Employing the JW transform, the diagonal terms can be written as

$$h_{pp} a_p^\dagger a_p = h_{pp} Q_{p'}^\dagger Q_{p'} = h_{pp}|1\rangle_{p'}\langle 0|_{p'}|0\rangle_{p'}\langle 1|_{p'} = h_{pp}|1\rangle_{p'}\langle 1|_{p'} = \frac{h_{pp}}{2}\left(I_{p'} - Z_{p'}\right). \tag{76}$$

For the exponential it holds

$$e^{-ih_{pp}a_p^\dagger a_p \delta t} = e^{\frac{-ih_{pp}\delta t}{2}} R_z(-h_{pp}\delta t)_{p'}. \tag{77}$$

Similarly, the off-diagonal terms read

$$h_{pq} a_p^\dagger a_q + h_{qp} a_q^\dagger a_p = \frac{h_{pq}}{2}\left[X_{p'} \otimes Z_{p'\to q'} \otimes X_{q'} + Y_{p'} \otimes Z_{p'\to q'} \otimes Y_{q'}\right], \tag{78}$$

where $Z_{p'\to q'}$ represents the direct product

$$Z_{p'\to q'} \equiv Z_{(p+1)'} \otimes Z_{(p+2)'} \otimes \ldots \otimes Z_{(q-2)'} \otimes Z_{(q-1)'}. \tag{79}$$

The exponential of the string of Z operators $\exp[-i\delta t(Z \otimes \ldots \otimes Z)]$ is in fact diagonal in the computational basis with the phase shift $e^{\pm i\delta t}$ on the diagonal. The sign of this phase shift depends on the parity of the corresponding basis state ("+" if the number of ones in the binary

representation is odd, "$-$" otherwise). The exponential can be implemented with the following circuit [9]

(80)
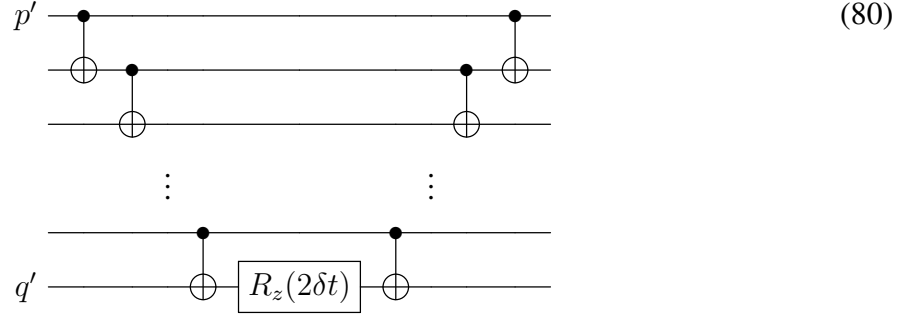
where CNOTs assure the correct sign of the phase shift according to the parity of the state and z-rotations were defined in Eq. (10). Generalization to the cases with X or Y operators acting on p' and q' qubits (Eq. (78)) can be easily realized with change-of-basis operators applied on p' and q' qubit before and after the action of the quantum circuit from Eq. (80). We have already shown in Eqs. (14) and (15) that, e.g., the Hadamard gate changes the basis from X to Z (and vice versa). The procedure for the two-electron part of the Hamiltonian is more elaborate, but completely analogous and can be found in [26].

The JW mapping is simple, but not the most economic one, when it comes to the number of gates required. As can be seen in Eq. (80), the quantum gates overhead scales as $\mathcal{O}(M)$. This is because the parity unlike the occupation of spin orbitals is not stored locally and must be collected by means of CNOT's before the single qubit rotation is applied. An alternative, which however has the same $\mathcal{O}(M)$ scaling, is the parity encoding. In this approach, the parity is stored locally and the occupation of spin orbitals non-locally

$$|o_1 \ldots o_M\rangle \to |q_M \ldots q_1\rangle, \qquad q_{p'} = \left[\sum_{i=1}^{p} o_i \right] (\mathrm{mod}\ 2).$$
(81)

The same scaling as for the JW mapping stems from the fact that when the occupation of a given orbital is changed, all the parities to which it contributes have to be updated, e.g. the first contributes to all of them.

More efficient than the JW mapping is the Bravyi-Kitaev (BK) mapping [27], which is a combination of the Jordan-Wigner and parity mappings. It compromises on the locality of occupation and parity information. The qubits store partial sums of occupation numbers, according to the BK matrix, β_{pq},

$$|o_1 \ldots o_M\rangle \to |q_M \ldots q_1\rangle, \qquad q_{p'} = \left[\sum_{q=1}^{p} \beta_{pq} o_q \right] (\mathrm{mod}\ 2),$$
(82)

which is defined recursively

$$\beta_1 = [1],$$
$$\beta_{2^{i+1}} = \begin{pmatrix} \beta_{2^i} & \mathbf{0} \\ \mathbf{A} & \beta_{2^i} \end{pmatrix},$$
(83)

where $\mathbf{A}$ is a $2^i \times 2^i$ matrix filled with zeros except the bottom row, which is filled with ones. For example for $M = 4$, the BK matrix reads

$$\beta_4 = \begin{pmatrix} 1 & 0 & 0 & 0 \\ 1 & 1 & 0 & 0 \\ 0 & 0 & 1 & 0 \\ 1 & 1 & 1 & 1 \end{pmatrix}. \tag{84}$$

The construction of second-quantized operators in the BK mapping is much more involved than in the JW mapping and we will not discuss it here, but rather refer readers to the work of Seeley *et al.* [28]. The ingenious BK mapping, which combines the occupation and parity as can be clearly seen from the structure of the BK matrix, Eq. (84), in fact leads to the $\mathcal{O}(\log_2 M)$ scaling. Recently, also more sophisticated mappings with certain advantages have been presented, e.g., generalizations of the BK mapping, which reduce the number of qubits due to symmetries (particle number, spin, or point group symmetries) [5].

5 Quantum algorithms for quantum chemistry

In this section, we will discuss the two main approaches which are cornerstones of most of the quantum algorithms for chemistry. In particular, the phase estimation which is an ultimate algorithm for error-corrected quantum devices with a potential to simulate very accurately the most complex molecular systems in future, and the variational quantum eigensolver, which combines the power of both quantum and classical computers and is suitable for NISQ devices.

5.1 Phase estimation

5.1.1 Phase estimation algorithm

The phase estimation algorithm (PEA) [9] is a quantum algorithm for obtaining an eigenvalue of a unitary operator U, based on a given initial guess of the corresponding eigenvector. Since a unitary U can be written as $U = e^{iH}$, with H Hermitian, the PEA can be viewed as a quantum substitute of the classical diagonalization.
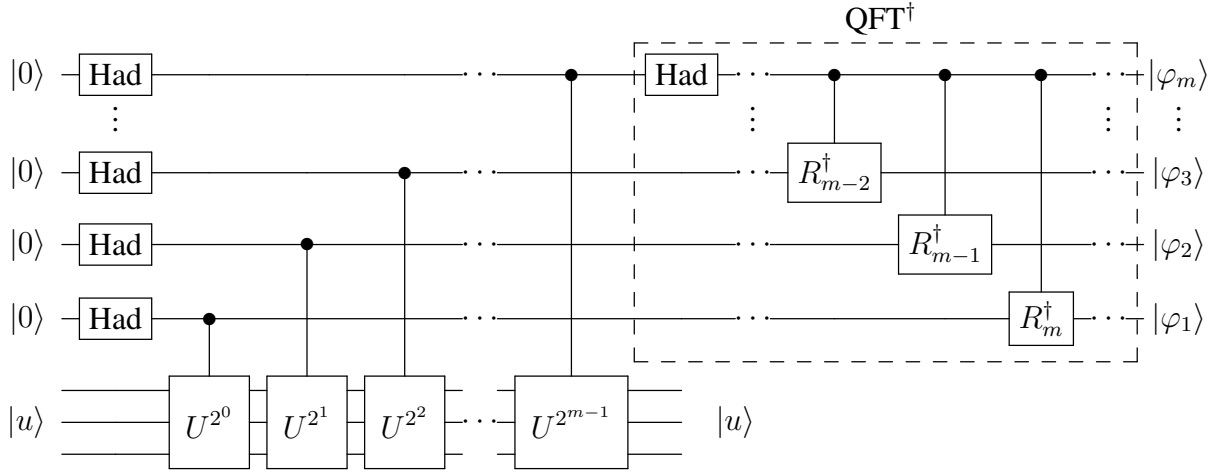Suppose that $|u\rangle$ is an eigenvector of U and that it holds

$$U|u\rangle = e^{2\pi i \varphi}|u\rangle, \qquad \varphi \in [0, 1), \tag{85}$$

where φ is the phase which is estimated by the algorithm. The quantum register is divided into two parts. The first one, called the read-out part, is composed of m qubits on which the binary representation of φ is measured at the end and which is initialized to the state $|0\rangle^{\otimes m}$. The second part contains the corresponding eigenvector $|u\rangle$.
The PEA quantum circuit is shown in Fig. 6. The application of Hadamard gates on all qubits in the first part of the register gives

$$|\text{reg}\rangle = \frac{1}{\sqrt{2^m}}\Big(|0\rangle + |1\rangle\Big) \dots \Big(|0\rangle + |1\rangle\Big)|u\rangle = \frac{1}{\sqrt{2^m}} \sum_{j=0}^{2^m-1} |j\rangle|u\rangle. \tag{86}$$

Fig. 6: *The PEA circuit with the highlighted part corresponding to the inverse quantum Fourier transform [9].*

Next, after the application of a sequence of controlled powers of U, the register is transformed into

$$|\text{reg}\rangle = \frac{1}{\sqrt{2^m}}\left(|0\rangle + e^{2\pi i 2^{m-1}\varphi}|1\rangle\right)\left(|0\rangle + e^{2\pi i 2^{m-2}\varphi}|1\rangle\right)\ldots\left(|0\rangle + e^{2\pi i 2^0\varphi}|1\rangle\right)|u\rangle$$

$$= \frac{1}{\sqrt{2^m}}\sum_{j=0}^{2^m-1} e^{2\pi i j\varphi}|j\rangle|u\rangle. \tag{87}$$

The crucial part of the PEA is the *efficient* inverse quantum Fourier transform (QFT†, highlighted in Fig. 6) performed on the read-out part of the register. The R_j operator is defined as [9]

$$R_j = \begin{pmatrix} 1 & 0 \\ 0 & e^{2\pi i/2^j} \end{pmatrix}. \tag{88}$$

If the phase can be expressed exactly with m bits

$$\varphi = 0.\varphi_1\varphi_2\ldots\varphi_m = \frac{\varphi_1}{2} + \frac{\varphi_2}{2^2} + \ldots + \frac{\varphi_m}{2^m}, \qquad \varphi_i \in \{0,1\}, \tag{89}$$

it (and consequently the eigenvalue) is recovered with unit probability by a measurement on the first part of the quantum register, which is by QFT† transformed into $|2^m\varphi\rangle$.

When the phase cannot be expressed exactly with m bits, in order to obtain this precision with the success probability of at least $1-\varepsilon$, one has to use n qubits [9]

$$n = m + \lceil \log_2(2 + 1/2\varepsilon)\rceil. \tag{90}$$

If the desired eigenvector is not known explicitly (as is typically the case in quantum chemistry), we can start the algorithm with an arbitrary initial guess vector $|\psi\rangle$, which can be expanded in terms of eigenvectors of U

$$|\psi_{\text{init}}\rangle = \sum_i c_i |u_i\rangle. \tag{91}$$

When using the number of ancillary qubits according to the Eq. (90), the success probability is decreased to $|c_i|^2(1-\varepsilon)$ (due to the linearity of quantum mechanics). It is therefore crucial for the success of the algorithm to be initialized with a wave function, which has a non-zero overlap with the exact targeted state. We will discuss some of the techniques of the initial state preparation in the following subsection.

We would like to note that the original phase estimation algorithm briefly sketched above has been improved in many aspects over the years. For example only one ancillary qubit can be used for sequential measurement of the phase. Also modifications for better efficiency, including parallelization or resistance to noise, have been proposed [6, 5].

5.1.2   Initial state preparation

Initial states with a large-enough overlap with the exact targeted state are key for the success of the phase estimation algorithm. In fact, a randomly chosen state from an exponentially large Hilbert space would have an exponentially decreasing overlap with the exact state, as the system size increases. This is indeed in agreement with the fact that solving the ground state problem of a completely general local Hamiltonian is a QMA-complete (quantum Merlin-Arthur complete, the quantum analogue of NP-complete) problem, i.e., considered difficult even for a quantum computer [29]. Nevertheless, the electronic structure problem of physically relevant systems, is believed to be *efficiently* solvable by means of quantum computers. In this case, the initial state preparation methods outlined below may be used.

Aspuru-Guzik *et al.* in their seminal work [8] proposed the adiabatic state preparation (ASP) algorithm inspired by the adiabatic model of quantum computing. In this approach, one slowly varies the Hamiltonian of the quantum register, starting with a trivial one and the register in its (exactly known) ground state, e.g. the Hartree-Fock state, and ending with the final exact one in the following simple way

$$H = (1 - t/T)H_{\text{init}} + (t/T)H_{\text{exact}} \qquad t : 0 \longrightarrow T, \tag{92}$$

where t is time and T the maximum annealing time. The efficiency of ASP depends on the minimum energy gap between the ground- and the first excited state along the adiabatic path, $g_{\min}$

$$g_{\min} = \min_{0 \leq s \leq 1} \big(E_1(s) - E_0(s)\big), \qquad s = t/T. \tag{93}$$

In particular, the maximum annealing time scales as

$$T \approx \mathcal{O}\left(\frac{M^4}{g_{\min}^2}\right). \tag{94}$$

Similarly to the phase estimation also ASP has been improved in several aspects. For example, non-linear adiabatic paths, more efficient for chemical problems, have been proposed and numerically tested [30].

Alternative options for the initial state preparation can be variational methods discussed in Sec. 5.2, or employing reference states obtained by some polynomially scaling computational methods. Several such methods including CI, CASSCF, selected CI, or tensor networks have already been used in numerical simulations [6].

5.1.3 Hamiltonian time evolution

If we take U in Eq. (85) in the form

$$U = e^{-iH\tau}, \tag{95}$$

where τ is a suitable parameter (equivalent to time in a time evolution) assuring φ being in the interval $[0,1)$ and H the electronic Hamiltonian, then the phase estimation algorithm reveals its energy spectrum. The whole procedure can be simply viewed as a time propagation of a trial wave function followed by the QFT switching from the time to energy domain and a measurement projecting out a certain eigenstate. Looking at the circuit in Fig. 6 and observing that the unitary U is applied up to the power 2^{n-1} and that the number of ancillary qubits is related to the precision according to Eq. (90), the total evolution time (the number of e^{-iH} calls) is proportional to $\mathcal{O}(1/\varepsilon)$. This number of calls governs the cost of a simulation. For the case of molecular Hamiltonians (Eq. (51)), Reiher *et al.* showed numerically that a number of calls scales as $\pi/2\varepsilon$ [23].

There are multiple ways how to implement the time evolution operator of the form e^{-iHt}. In Sec. 2.2, we have already mentioned the first-order Trotter approximation, Eq. (18). In order to achieve accuracy ε, the number of Trotter steps $N = \mathcal{O}(t^2/\varepsilon)$. This can be improved by using higher order product formulae. It was also shown that the accuracy can be further improved by, e.g., randomly ordering the terms in the Trotter sequence [5]. The gate counts of all Trotter-based approaches scale as $\mathcal{O}(\mathrm{poly}(1/\varepsilon))$.

Several more advanced methods for time evolution, which are more efficient than Trotterization have been proposed [6]. Description of these approaches is, however, beyond the scope of this chapter. We will only briefly mention the Taylor series method, in which the Hamiltonian evolution, Eq. (95), is divided into shorter segments and each of the segment exponentials is approximated by a truncated Taylor series, which can be expanded as a linear combination of unitaries (LCU). These unitaries are then applied in a superposition employing oracle circuits. For a detailed summary of different Hamiltonian simulation techniques and references to original papers, we refer readers to the review [6].

In order to study the asymptotic scaling of the phase estimation based algorithms, one typically employs the fixed chemical accuracy. The scaling properties largely depend on the basis set employed, i.e., number of terms in the Hamiltonian (as discussed in Sec.3.1) as well as the actual algorithm used for implementation of the Hamiltonian time evolution (Eq. (95)). In the Gaussian basis, the second quantized Hamiltonian contains $\mathcal{O}(M^4)$ terms and the Taylor series method, which is more sophisticated than the Trotter based approaches, scales as $\mathcal{O}(M^5)$ [5]. On the other hand, it is well known that rigorous bounds on the Trotter error are loose by several orders of magnitude. In the plane wave dual basis, the Hamiltonian contains $\mathcal{O}(M^2)$ terms and the Taylor series method was shown to scale as $\mathcal{O}(M^{2.67})$ [5]. We would like to note, however, that more advanced Hamiltonian simulation techniques, which were not discussed here, can lead to even lower scaling. For example in the plane wave basis, algorithms which achieve sublinear scaling in M have been developed.

In spite of the recent development of highly sophisticated algorithms for Hamiltonian simula-
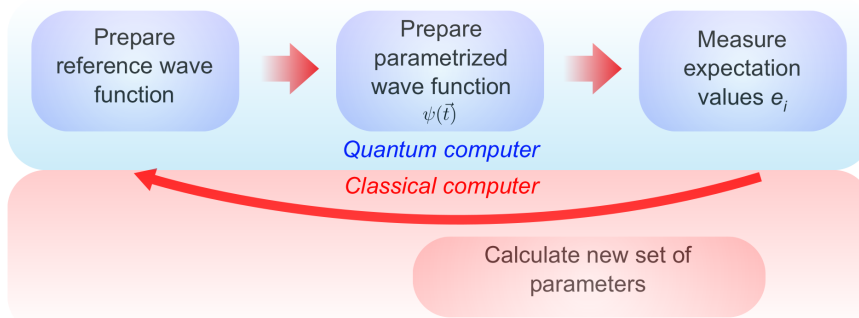
Fig. 7: *Flow chart of the variational quantum eigensolver.*

tions, the phase estimation based approaches require quantum circuits with a large number of gates, which are expected to require some form of a quantum error correction. Therefore they are not suitable for near term devices, which will not have enough qubits for this purpose.

5.2 Variational quantum-classical algorithms

A promising alternative to the phase estimation for near-term quantum devices is the variational quantum eigensolver (VQE) approach [31, 32], which combines classical variational energy minimization over normalized trial wave functions $\Psi(\vec{\vartheta})$

$$E = \min_{\vec{\vartheta}} \left\langle \Psi(\vec{\vartheta}) \middle| H \middle| \Psi(\vec{\vartheta}) \right\rangle \tag{96}$$

with a state preparation and a measurement of the Hamiltonian expectation value on a quantum computer. The VQE method in fact trades long coherent quantum circuits for short circuits and lots of measurements (though at the cost of asymptotically worse scaling in terms of precision). The scheme of VQE is depicted in Fig. 7.

The starting point of VQE is a preparation of the fixed reference state $|\Psi_{\mathrm{ref}}\rangle$, which can be the Hartree-Fock determinant or also some multireference state. Then for an initial set of a polynomial number of parameters $\vec{\vartheta}$, a series of parametrized gates $U(\vec{\vartheta})$ (ansatz circuit) is applied on $|\Psi_{\mathrm{ref}}\rangle$, producing the so called ansatz state $\left|\Psi(\vec{\vartheta})\right\rangle$. Here comes the advantage of quantum hardware, since ansatz states cannot be stored and manipulated on a classical computer for general $U(\vec{\vartheta})$ (due to the exponentially large Hilbert space). We will discuss different types of ansatz circuits below.

After preparing the ansatz state, the expectation value of the Hamiltonian is measured. We are working with the second-quantized representation and we have already shown in Sec. 4.2 that when employing the JW transformation (or the BK one), the Hamiltonian is mapped to a linear combination of products of Pauli operators, as shown in Eq. (74). The energy can be written as

$$E(\vec{\vartheta}) = \sum_j h_j \left\langle \Psi(\vec{\vartheta}) \middle| \prod_i \sigma_i^j \middle| \Psi(\vec{\vartheta}) \right\rangle, \tag{97}$$

where, as in Eq. (74), σ_i^j stands for one of the Pauli operators (X, Y, Z) or the identity acting on the ith qubit, the sum over j runs over all one and two-electron terms and h_j formally represent one and two-electron integrals. In the Hamiltonian averaging method [32], each term is

repeatedly measured (each time the ansatz state must be prepared) in order to get the desired precision. This approach requires $\mathcal{O}(1/\varepsilon^2)$ measurements to get the energy with precision ε.

The measured energy is then together with the actual values of $\vec{\vartheta}$ passed to a classical optimization routine. This can be a gradient-free optimization, such as Nelder-Mead simplex, or some gradient-descent, since strategies to directly measure the energy gradients with respect to one of the parameters were also developed [5]. The classical optimization produces a new set of parameters $\vec{\vartheta}$ and the whole procedure is repeated until energy convergence.

The advantage of VQE over classical computational methods certainly depends on the employed ansatz. Two types of ansätze have been used so far. The first category are so called hardware efficient ansätze and it comprises the limited parametrized gate set, which is easy to implement on a given quantum architecture. The aim is to produce as much flexible ansatz state as possible with a minimal number of gates. These approaches do not use any information about a system studied, however, have been successfully demonstrated on several small molecules [5].

The second category comprises chemically inspired ansätze. To the best of our knowledge, all VQE methods of this type are based on the unitary coupled cluster theory (Sec. 3.3.2) usually restricted up to double excitations and employ

$$U(\vec{\vartheta}) = e^{T-T^{\dagger}}. \tag{98}$$

The point is that the UCCSD method cannot be performed *efficiently* on a classical computer due to infinite commutator expansions, as discussed in Sec. 3.3.2, but it can be implemented on a quantum computer. The CC amplitudes are then the VQE variational parameters. Moreover, the fully variational UCCSD method is expected to outperform traditional CCSD in accuracy [32] and converge even for multireference problems.

Since T and $T^{\dagger}$ in Eq. (98) do not commute, some sort of numerical approximation similar to those used in the Hamiltonian time evolution (Sec. 5.1.3) has to be used in order to implement the circuit ansatz by means of single and two-qubit gates. If we assume that we have a reasonable $|\Psi_{\text{ref}}\rangle$, which is close enough to the exact state, the CC amplitudes are expected to be small numbers (much smaller than 1). In this case, much less Trotter steps are necessary than for the phase estimation based approaches. In fact, it was shown that even a single Trotter step can be used to implement the circuit ansatz from Eq. (98), which yields accurate results [5]. In this case, the number of quantum gates for the UCCSD circuit ansatz implementation scales as $\mathcal{O}(M^3 N^2)$ when the JW mapping is employed [$\mathcal{O}(M^2 N^2 \log_2 M)$ for the BK mapping].

Undoubtedly, the biggest bottleneck of VQE is the huge number of measurements (requiring repeated state preparation) in the Hamiltonian averaging method. It was shown [32] that the number of measurements N_m required to estimate the energy with precision ε is bounded by

$$N_m = \frac{\left(\sum_i |h_i|\right)^2}{\varepsilon^2}, \tag{99}$$

where h_i again represent one and two-electron integrals. The number of measurements thus scales as $\mathcal{O}(M^8/\varepsilon^2)$ in a Gaussian basis, which can be reduced by using local basis sets to $\mathcal{O}(M^6/\varepsilon^2)$, and $\mathcal{O}(M^4/\varepsilon^2)$ in a plane wave dual basis [6]. However, as in the case of the phase

estimation based approaches, advanced techniques, whose presentation is behind the scope of this chapter, have been developed, which reduce this scaling in certain cases by orders of magnitude [5].

The VQE method has also been extended for excited state calculations. One such approach is the quantum subspace expansion (QSE) of McClean *et al.* [33], in which a polynomial number of additional measurements allows the treatment of excited states. In this method, excited states are expanded in a subspace around the ground state $|\Psi_0\rangle$ spanned by single excitations $a_p^\dagger a_q |\Psi_0\rangle$ for all possible p, q. They can be found by solving the generalized eigenvalue problem

$$H^{\text{QSE}}C = S^{\text{QSE}}CE, \tag{100}$$

where C is a matrix of eigenvectors, E a diagonal matrix of energies and the Hamiltonian matrix H^{QSE} is given by

$$H^{\text{QSE}}_{pq,rs} = \langle \Psi_0 | a_p a_q^\dagger H a_r^\dagger a_s | \Psi_0 \rangle. \tag{101}$$

Since the subspace states are not orthogonal, the overlap matrix has to be also obtained

$$S^{\text{QSE}}_{pq,rs} = \langle \Psi_0 | a_p a_q^\dagger a_r^\dagger a_s | \Psi_0 \rangle. \tag{102}$$

One can see in Eq. (100) that this approach of excited state calculations requires, on top of measuring the one-particle and two-particle reduced density matrices (1-RDMs, 2RDMs), which are measured in standard VQE,[5] also measuring the 3-RDMs and 4-RDMs.

6 Summary

In this chapter, we have reviewed some of the basic concepts, which were developed for the simulation of chemical problems on quantum computers. In fact, quantum computational chemistry [5] has achieved enormous progress recently and it would be impossible to include all important developments in this field. On the small illustrative examples, we have rather shown the basic strategies, which may be used also in case of more advanced algorithms.

We have presented how to map the quantum chemistry problems onto a register of qubits both in the first and second quantization and most of the time restricted ourselves to the electronic structure problem. The two main approaches to this problem have been discussed: the phase estimation algorithm, which is an ultimate algorithm for error-corrected quantum devices as well as the variational quantum eigenvalue solver, which combines power of both quantum and classical computers and is due to short quantum circuits suitable for near-term devices.

---

[5]These are indeed the individual expectation values in Eq. (97)

References

[1] R.P. Feynman, Int. J. Theor. Phys. **21**, 467 (1982)

[2] F. Arute, K. Arya, R. Babbush, D. Bacon, J.C. Bardin, R. Barends, R. Biswas, S. Boixo, F.G.S.L. Brandao, D.A. Buell, B. Burkett, Y. Chen, Z. Chen, B. Chiaro, R. Collins, W. Courtney, A. Dunsworth, E. Farhi, B. Foxen, A. Fowler, C. Gidney, M. Giustina, R. Graff, K. Guerin, S. Habegger, M.P. Harrigan, M.J. Hartmann, A. Ho, M. Hoffmann, T. Huang, T.S. Humble, S.V. Isakov, E. Jeffrey, Z. Jiang, D. Kafri, K. Kechedzhi, J. Kelly, P.V. Klimov, S. Knysh, A. Korotkov, F. Kostritsa, D. Landhuis, M. Lindmark, E. Lucero, D. Lyakh, S. Mandrà, J.R. McClean, M. McEwen, A. Megrant, X. Mi, K. Michielsen, M. Mohseni, J. Mutus, O. Naaman, M. Neeley, C. Neill, M.Y. Niu, E. Ostby, A. Petukhov, J.C. Platt, C. Quintana, E.G. Rieffel, P. Roushan, N.C. Rubin, D. Sank, K.J. Satzinger, V. Smelyanskiy, K.J. Sung, M.D. Trevithick, A. Vainsencher, B. Villalonga, T. White, Z.J. Yao, P. Yeh, A. Zalcman, H. Neven, and J.M. Martinis, Nature **574**, 505 (2019)

[3] H.S. Zhong, H. Wang, Y.H. Deng, M.C. Chen, L.C. Peng, Y.H. Luo, J. Qin, D. Wu, X. Ding, Y. Hu, P. Hu, X.Y. Yang, W.J. Zhang, H. Li, Y. Li, X. Jiang, L. Gan, G. Yang, L. You, Z. Wang, L. Li, N.L. Liu, C.Y. Lu, and J.W. Pan, Science **370**, 1460 (2020)

[4] J. Preskill, Quantum **2**, 79 (2018)

[5] S. McArdle, S. Endo, A. Aspuru-Guzik, S.C. Benjamin, and X. Yuan, Rev. Mod. Phys. **92**, 015003 (2020)

[6] Y. Cao, J. Romero, J.P. Olson, M. Degroote, P.D. Johnson, M. Kieferová, I.D. Kivlichan, T. Menke, B. Peropadre, N.P.D. Sawaya, S. Sim, L. Veis, and A. Aspuru-Guzik, Chem. Rev. **119**, 10856 (2019)

[7] K. Head-Marsden, J. Flick, C.J. Ciccarino, and P. Narang, Chem. Rev. **121**, 3061 (2020)

[8] A. Aspuru-Guzik, A.D. Dutoi, P.J. Love, and M. Head-Gordon, Science **309**, 1704 (2005)

[9] M.A. Nielsen and I.L. Chuang: *Quantum Computation and Quantum Information* (Cambridge University Press, 2000)

[10] I. Buluta and F. Nori, Science **326**, 108 (2009)

[11] S. Lloyd, Science **273**, 1073 (1996)

[12] D.S. Abrams and S. Lloyd, Phys. Rev. Lett. **79**, 2586 (1997)

[13] N. Hatano and M. Suzuki: *Finding Exponential Product Formulas of Higher Orders*, in *Lecture Notes in Physics* (Springer, Heidelberg, 2005)

[14] Y. Li and S.C. Benjamin, Phys. Rev. X **7** (2017)

[15] D.S. Abrams and S. Lloyd, Phys. Rev. Lett. **83**, 5162 (1999)

[16] I. Kassal, S.P. Jordan, P.J. Love, M. Mohseni, and A. Aspuru-Guzik,
Proc. Natl. Acad. Sci. U.S.A **105**, 18681 (2008)

[17] L. Veis, J. Višňák, H. Nishizawa, H. Nakai, and J. Pittner,
Int. J. Quantum Chem. **116**, 1328 (2016)

[18] A. Szabo and N.S. Ostlund: *Modern quantum chemistry* (MacMillan, New York, 1982)

[19] B.P. Pritchard, D. Altarawy, B. Didier, T.D. Gibson, and T.L. Windus,
J. Chem. Inf. Modeling **59**, 4814 (2019)

[20] R. Babbush, N. Wiebe, J. McClean, J. McClain, H. Neven, and G.K.L. Chan,
Phys. Rev. X **8** (2018)

[21] J. Gauss: In P. v. R. Schleyer, N.L. Allinger, T. Clark, J. Gasteiger, P.A. Kollman,
H.F. Schaefer III, and P.R. Scheiner (eds.) *The Encyclopedia of Computational Chemistry*
(Wiley, Chichester, 1998), pp. 615–636

[22] D.I. Lyakh, M. Musiał, V.F. Lotrich, and R.J. Bartlett, Chem. Rev. **112**, 182 (2011)

[23] M. Reiher, N. Wiebe, K.M. Svore, D. Wecker, and M. Troyer,
Proc. Natl. Acad. Sci. U.S.A. **114**, 7555 (2017)

[24] A.G. Taube and R.J. Bartlett, Int. J. Quantum Chem. **106**, 3393 (2006)

[25] P. Jordan and E. Wigner, Z. Phys. A **47**, 631 (1928)

[26] J.D. Whitfield, J. Biamonte, and A. Aspuru-Guzik, Mol. Phys. **109**, 735 (2011)

[27] S.B. Bravyi and A.Y. Kitaev, Ann. Phys. **298**, 210 (2002)

[28] J.T. Seeley, M.J. Richard, and P.J. Love, J. Chem. Phys. **137**, 224109 (2012)

[29] J. Kempe, A. Kitaev, and O. Regev, SIAM J. Comput. **35**, 1070 (2006)

[30] L. Veis and J. Pittner, J. Chem. Phys. **140**, 214111 (2014)

[31] A. Peruzzo, J. McClean, P. Shadbolt, M.H. Yung, X.Q. Zhou, P.J. Love, A. Aspuru-Guzik,
and J.L. O'Brien, Nat. Commun. **5** (2014)

[32] J.R. McClean, J. Romero, R. Babbush, and A. Aspuru-Guzik,
New J. Phys. **18**, 023023 (2016)

[33] J.R. McClean, M.E. Kimchi-Schwartz, J. Carter, and W.A. de Jong, Phys. Rev. A **95** (2017)